Propagation Buckling in Subsea Pipe-in-Pipe Systems

Author

Karampour, Hassan, Alrsai, Mahmoud, Albermani, Faris, Guan, Hong, Jeng, Dong-Sheng

Published

2017

Journal Title

Journal of Engineering Mechanics

Version

Accepted Manuscript (AM)

DOI

10.1061/(ASCE)EM.1943-7889.0001337

Propagation Buckling in Subsea Pipe-in-pipe Systems

Hassan Karampour[1]; Mahmoud Alrsai[2]; Faris Albermani[3];
Hong Guan[4]; and Dong-Sheng Jeng, M.ASCE[5]

Abstract: This study investigates buckle propagation of subsea pipe-in-pipe (PIP) systems under hydrostatic pressure. Unlike in previous studies, PIP systems consisting of carrier pipes with a diameter-to-thickness (D_o/t_o) ratio in the range 26–40 are examined here. Experimental results from ring squash tests (RSTs), confined ring squash tests (CRSTs), and hyperbaric chamber tests are presented and compared with a modified two-dimensional (2D) analytical solution and with numerical results using three-dimensional (3D) finite-element (FE) analysis. The comparison indicates that the proposed modified analytical expression provides a more accurate lower-bound estimate of the propagation buckling pressure of PIP systems compared with the existing equations, especially for higher D_o/t_o ratios. The novel RST and CRST protocols proposed for PIP systems give lower-bound estimates of the propagation pressure. The FE analysis outcomes demonstrate that the lengths of PIP system transition zones are almost twice the corresponding lengths in single pipes. New modes of buckling are discovered in the hyperbaric chamber tests of PIP systems with $D_o/t_o = 26$. **DOI: 10.1061/(ASCE)EM.1943-7889.0001337.**

Author keywords: Pipe-in-pipe systems; Propagation buckling; Confined buckling; Ring squash test.

Introduction

Pipe-in-pipe (PIP) systems are being used extensively in the design of high-pressure and high-temperature (HP/HT) flowlines because of their outstanding thermal insulation. A typical PIP system consists of concentric inner and outer pipes, bulkheads, and centralizers. The inner pipe (flowline) conveys production fluids, and the outer pipe (carrier pipe) protects the system from external pressure and mechanical damage. These two pipes are isolated by centralizers at joints and connected through bulkheads at both ends of the pipeline. The annulus (the space between the tubes) is either empty or filled with nonstructural insulation material such as foam or water (Bai and Bai 2005).

Pipe-in-Pipe systems are normally divided into two categories: compliant and noncompliant. In a compliant system, the inner pipe and the carrier pipe are attached at close intervals; in a noncompliant system, the pipes are connected only through bulkheads at discrete locations. The relative movement between the inner and outer pipes is arrested in a compliant system, whereas the two pipes can move relative to each other in a noncompliant system. Pipe-in-Pipe systems are exploited in subsea developments, where the carrier pipe is designed to resist high hydrostatic pressures (water depths up to 3,000 m) and the inner pipe is designed to transmit hydrocarbons at temperatures as high as 180°C (Jukes et al. 2009). The HP/HT flow can cause global upheaval (Wang et al. 2015) or lateral buckling (Vaz and Patel 1999) in the system. Furthermore, high hydrostatic pressure may trigger a local collapse in the carrier pipe, such as propagation buckling or buckle interaction (Karampour et al. 2013; Karampour et al. 2013; Karampour and Albermani 2014, 2015; Karampour et al. 2015). The structural integrity of the PIP system under external pressure is an issue of concern because the collapse of the carrier pipe may result in the collapse of the inner pipe.

In a single pipeline under external pressure, a local dent or ovalization in the pipe wall can initiate a buckle that rapidly transforms the pipe cross section into a dog-bone shape. The buckle then travels along the pipeline as long as the external pressure is high enough to sustain propagation. The lowest pressure required to perpetuate the buckle is termed *propagation pressure*, P_p, which is only a fraction of the buckle initiation pressure. The collapse and propagation of buckling in single pipelines have been extensively investigated using analytical, experimental, and numerical methods. Most notable are the early analytical studies by Mesloh et al. (1973) and Palmer and Martin (1975) and the experimental and numerical investigations by Kyriakides and Babcock (1981) and Albermani et al. (2011). Recently Karampour et al. (2013) and Karampour and Albermani (2014) investigated the possible interaction between global buckling of water pipelines, such as upheaval and lateral buckling (Karampour et al. 2013), and propagation buckling. They suggested a novel design for ultradeep pipelines (Karampour and Albermani 2015; Karampour et al. 2015) that increases the propagation buckling capacity of the pipeline without increasing wall thickness.

Despite extensive investigations performed on the integrity of single pipelines, to date PIP instabilities have only been marginally addressed. Kyriakides (2002) conducted a thorough experimental study on propagation buckling of steel PIP systems with 2-in.-diameter carrier tubes with diameter-to-thickness (D_o/t_o) ratio values of 24.1, 21.1, and 16.7 and inner pipes with various diameter-to-thickness (D_i/t_i) ratio values ranging between 15 and 37. Kyriakides (2002) observed two dominant modes of buckling.

[1]Lecturer, Griffith School of Engineering, Griffith Univ., Gold Coast Campus, Southport, QLD 4222, Australia (corresponding author). E-mail: h.karampour@griffith.edu.au

[2]Ph.D. Student, Griffith School of Engineering, Griffith Univ., Gold Coast Campus, Southport, QLD 4222, Australia.

[3]Associate Professor, School of Civil Engineering, Univ. of Queensland, St. Lucia, QLD 4072, Australia.

[4]Professor, Griffith School of Engineering, Griffith Univ., Gold Coast Campus, Southport, QLD 4222, Australia.

[5]Professor, Griffith School of Engineering, Griffith Univ., Gold Coast Campus, Southport, QLD 4222, Australia.

Note. This manuscript was submitted on August 1, 2016; approved on April 19, 2017No Epub Date. Discussion period open until 0, 0; separate discussions must be submitted for individual papers. This paper is part of the ***Journal of Engineering Mechanics***, © ASCE, ISSN 0733-9399.

Table 1. Properties of PIP Systems

Identifier	Carrier pipe	Inner pipe	D_o/t_o	D_i/t_i	D_i/D_o	t_i/t_o	E (MPa)	$\frac{E'}{E}(\%)$	σ_{Yo} (MPa)	$\frac{\sigma_{Yi}}{\sigma_{Yo}}$
PIP-1	$OD = 80$, $t = 2$	$OD = 40$, $t = 1.6$	40.0	25.0	0.50	0.80	69,000	1.01	169	0.93
PIP-2	$OD = 60$, $t = 2$	$OD = 40$, $t = 1.6$	30.0	25.0	0.75	0.80	69,000	0.97	139	1.12
PIP-3	$OD = 80$, $t = 3$	$OD = 40$, $t = 1.6$	26.7	25.0	0.50	0.53	69,000	1.02	209	0.75

Note: All dimensions are in millimeters; OD = outer diameter; t = thickness.

In the first mode, local collapse of the outer pipe led to simultaneous collapse of the inner pipe, whereas in the second mode the carrier pipe collapsed without affecting the inner pipe. Based on their experimental study and three-dimensional (3D) finite-element (FE) analyses, Kyriakides and Vogler (2002) suggested an empirical formula for PIP buckle propagation pressure, P_{p2}. Gong and Li (2015) carried out a finite-element study of propagation buckling of PIP systems with carrier pipes having D_o/t_o values of 25, 20, and 15 and inner tubes having D_i/t_i values of 15 and 20. Although both studies (Gong and Li 2015; Kyriakides and Vogler 2002) covered similar carrier pipe D_o/t_o ranges, two different empirical expressions were suggested.

Previous studies have focused on propagation buckling of PIP systems having carrier pipes with low D/t values. For a subsea pipeline, the use of buckle arrestors (Lee and Kyriakides 2004) is more economical than the use of a carrier pipe with a thick wall (low D_o/t_o value) to resist propagation buckling. The self-weight of the PIP system has to be kept low to ensure that the pipeline is installable. Increasing the wall thickness of the carrier pipe also significantly amplifies the axial force developed in the PIP system due to the internal pressure and temperature which in turn raises the risk of upheaval and lateral buckling in the system (Bokaian 2004). To address the aforementioned issues, the current study aims to investigate the collapse modes and buckle propagation pressures of PIP systems (see Table 1) with carrier pipes having higher D_o/t_o values than those in Gong and Li (2015) and Kyriakides and Vogler (2002).

A lower-bound analytical solution for PIP system propagation pressure is proposed herein. Hyperbaric chamber tests are conducted on 1.6-m aluminum (Al-6060-T5) PIP systems. Ring squash test (RST) and confined ring squash test (CRST) protocols are proposed to provide estimates of propagation pressure in the PIP systems with respect to buckling modes observed in the experiments. The paper concludes with a discussion of the FE results with emphasis on failure modes.

Analytical Solution of Propagation Pressure

Numerous analytical solutions have been suggested to estimate the propagation pressure of a single pipe. Unlike propagation pressure, initiation pressure is very sensitive to initial imperfections such as local dents or ovalizations. Propagation pressure is related to the plastic properties of the pipe and is only a fraction of the buckle initiation pressure. Both buckle initiation pressure and buckle propagation pressure are related to the pipe's ratio of diameter to wall thickness; however, previous studies have suggested that there is no evident relationship between the two (Albermani et al. 2011; Mesloh et al. 1973). The simplest propagation pressure model was established by Palmer and Martin (1975), which only considered the initial and final configurations of the pipe cross section. Fig. 1(a) shows the four plastic hinges developed in the pipe at different stages of propagation buckling. Palmer and Martin assumed a rigid–perfectly plastic material with yield stress σ_{Yo}. By equating

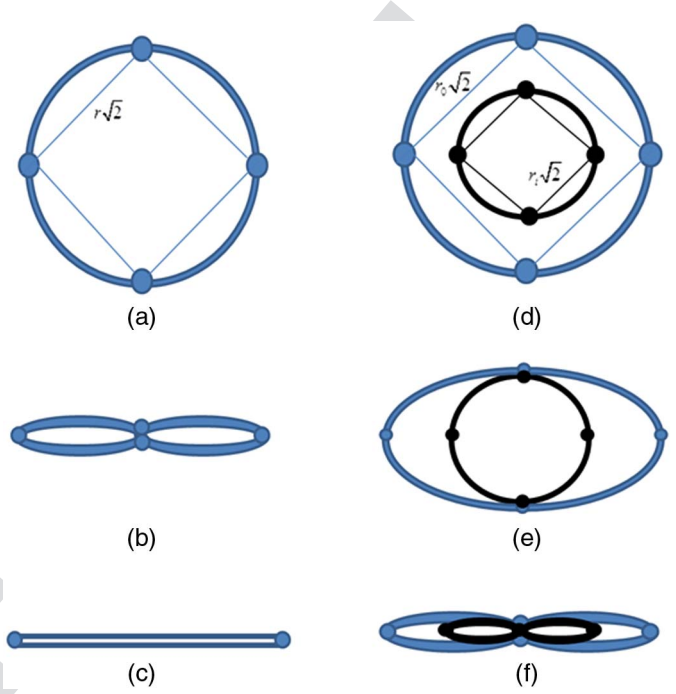

Fig. 1. Schematic of deformation stages in propagation buckling: (a–c) single pipe; (d–f) pipe-in-pipe system

the plastic work expanded in the four hinges (internal work) to the work done by hydrostatic pressure due to the change in pipe volume, they found the following expression for single-pipe propagation pressure (P_p):

$$\overline{P_p} = \pi\sigma_{Yo}\left(\frac{t_o}{D_o}\right)^2 \tag{1}$$

where D_o and t_o = outside diameter and wall thickness of the carrier pipe, respectively. Experimental studies (Albermani et al. 2011; Kyriakides and Babcock 1981) showed that Eq. (1) underestimates the propagation pressure of the pipeline, specifically at lower D/t values. Considering the collapse under the plane strain condition, propagation buckling of a single pipe can be expressed as (Chater and Hutchinson 1984; Kyriakides et al. 1984)

$$\hat{P}_p = \frac{2\pi}{\sqrt{3}}\sigma_{Yo}\left(\frac{t_o}{D_o}\right)^2 \tag{2}$$

Kyriakides and Vogler (2002) investigated the collapse of PIP systems using the plane strain condition and adopting a four-hinge mechanism in the carrier pipe and in the inner pipes. They considered the strain-hardening behavior in the material model of the plastic hinges and proposed the following expression for PIP propagation pressure:

$$\hat{P}_{p2} = \frac{2\pi}{\sqrt{3}}\sigma_{Yo}\left(\frac{t_o}{D_o}\right)^2\left[1 + \frac{\sigma_{Yi}}{\sigma_{Yo}}\left(\frac{t_i}{t_o}\right)^2\right] \quad (3)$$

where subscripts o and i = outer pipe and inner pipe, respectively. Albermani et al. (2011) proposed a modification to the lower-bound Palmer and Martin (1975) solution by accounting for both the circumferential membrane and the flexural effects in the pipe wall

$$W_{ex} = (W_{\text{in}})_f + (W_{\text{in}})_m \quad (4)$$

where W_{ex} = external work done by the net hydrostatic pressure; and W_{in} = internal work due to the circumferential flexure, f, and membrane, m, effects. The initially circular cross section of the pipe [Fig. 1(a)] deforms into a dog-bone [Fig. 1(b)] and eventually a nearly flat segment [Fig. 1(c)]. Accordingly, Eq. (4) can be written as

$$\tilde{P}_p(\Delta A) = 3\pi m_p + (pr)(\Delta l) \quad (5a)$$

where ΔA = change in cross-sectional area [Fig. 1(a–c)]; Δl = change in circumferential length; and m_p = plastic moment; these are given by

$$\Delta A = \pi r^2 \quad (5b)$$

$$\Delta l = 2\pi r - 4r\sqrt{2} = 0.626r \quad (5c)$$

$$m_p = \sigma_Y \frac{t^2}{4} \quad (5d)$$

Substituting Eqs. (5*b*) and (5*c*) into Eq. (5*a*), the propagation pressure, $\tilde{P}_p$, is obtained as

$$\tilde{P}_p = \frac{3}{2.515}\left[\pi\sigma_Y\left(\frac{t}{D}\right)^2\right] \quad (6)$$

The values of $\hat{P}_p$ and $\tilde{P}_p$ suggest a 15 and a 19% increase, respectively, in the propagation pressure of the single pipe compared with Palmer and Martin's (1975) expression, $\overline{P_p}$, regardless of the D/t value of the pipe.

The analytical lower-bound solution to propagation buckling of a single pipe given by Eq. (6) can be extended to pipe-in-pipe systems by accounting for the membrane and flexural effects of the outer and the inner pipes

$$W_{ex}^{\text{PIP}} = (W_{\text{in}})_f^{\text{PIP}} + (W_{\text{in}})_m^{\text{PIP}} \quad (7)$$

where W_{ex} = external work done by hydrostatic pressure; and W_{in} = internal work due to circumferential flexure, f, and membrane, m, effects. Based on experimental observations from hyperbaric chamber and ring squash tests, the initially circular cross section of the outer pipe [Fig. 1(d)] has been shown to deform into the shape in Fig. 1(e). Further increase in external pressure causes the PIPsystem to eventually deform into the dog-bone shape [Fig. 1(f)]. Thus Eq. (7) can be written as

$$\tilde{P}_{p2}(\Delta A) = 3\pi(m_{po} + m_{pi}) + \tilde{P}_{p2}(r_o.\Delta l_o + r_i.\Delta l_i) \quad (8a)$$

where ΔA = change in cross-sectional area; Δl = change in circumferential length; and m_p = plastic moment (Albermani et al. 2011); these are given by

$$\Delta A = \pi r_o^2 \quad (8b)$$

$$\Delta l_o = 0.626r_0; \qquad \Delta l_i = 0.626r_i \quad (8c)$$

Table 2. Comparison of Hyperbaric Chamber, Analytical, RST, and FE Results

	Hyperbaric chamber		Analytical				RST	FE
Identifier	P_p (kPa)	P_{p2} (kPa)	$\frac{\hat{P}_p}{P_p}$	$\frac{\hat{P}_{p2}}{P_{p2}}$	$\frac{\tilde{P}_p}{P_p}$	$\frac{\tilde{P}_{p2}}{P_{p2}}$	$\frac{P_{p2}^{\text{RST}}}{P_{p2}}$	$\frac{P_{p2}^{\text{FE}}}{P_{p2}}$
PIP-1	700	780	0.55	0.78	0.56	0.86	0.76	1.28
PIP-2	900	1,620	0.62	0.59	0.64	0.69	0.49	0.86
PIP-3	1,400	2,020[a]	0.76	0.64	0.79	0.66	0.49[b]–0.98[c]	0.96

[a]Corresponds to dog-bone buckle shape shown in Fig. 5(a).
[b]Dog-bone buckle shape.
[c]U-shape buckle.

$$m_{po} = \sigma_{Yo}\frac{t_o^2}{4}; \qquad m_{pi} = \sigma_{Yi}\frac{t_i^2}{4} \quad (8d)$$

where subscript o = outer pipe; and subscript i = inner pipe. Substituting Eqs. (8*b*)–(8*d*) into Eq. (8*a*), the propagation pressure, $\tilde{P}_{p2}$, of the PIP system is obtained as

$$\tilde{P}_{p2} = \left[\frac{3\pi\sigma_{Yo}}{2.515}\left(\frac{t_o}{D_o}\right)^2\right]\left[1 + \frac{\sigma_{Yi}}{\sigma_{Yo}}\left(\frac{t_i}{t_o}\right)^2\right]\left[\frac{1}{1 - (\frac{D_i}{2D_0})^2}\right] \quad (9)$$

When $D_i = t_i = 0$, Eq. (9) yields the propagation pressure of a single pipe as given by Eq. (6). Unlike Eq. (3), Eq. (9) accounts for the effect of D_i/D_o along with that of t_i/t_o and σ_i/σ_o.

Propagation buckling pressures of single pipes (outer pipes) and PIP systems determined from the analytical expressions in Eqs. (2), (3), (6), and (9) are listed in Table 2 and compared with the experimental results (P_p for a single pipe and P_{p2} for a PIP system) obtained from the hyperbaric chamber tests.

Hyperbaric Chamber Tests

The experimental protocol comprises end-sealing concentric PIP systems, with parameters given in Table 1 and a length of 1.6 m ($L/D > 20$), pressurized inside the hyperbaric chamber shown in Fig. 2. The chamber has an inner diameter of 173 mm and a length of 4 m and is rated for a working pressure of 20 MPa (2,000-m water depth). The intact PIP system was sealed at both ends by gluing on thick aluminum disks to ensure that the inner pipe was completely sealed from the outer pipe. Two valves were connected to each end of the PIP system, one on the carrier pipe and the other on the inner pipe. One valve was used for bleeding the pipe while filling it with water. The second valve was used to vent the carrier and inner pipes and to collect water from the inner pipe and the cavity between the inner and outer pipes during buckle propagation [through the hoses shown in Fig. 2(b)]. Volume-controlled pressurization with a high-pressure pump [shown in Fig. 2(a)] was used, and the pressure was increased until collapse of the system due to external pressure under quasi-static steady-state conditions. By maintaining a low rate of pumping, the chamber pressure was stabilized at propagation pressure, P_{p2}, with buckling longitudinally propagating along the PIP system sample accompanied by water flow from the vents. The change in volume of the system (ΔV) during the test was calculated by measuring the weight of water being discharged from the inner pipe and the cavity between the pipes separately using the digital weighing scales shown in Fig. 2(a). Control tests using a single pipe (outer pipe) were conducted first.

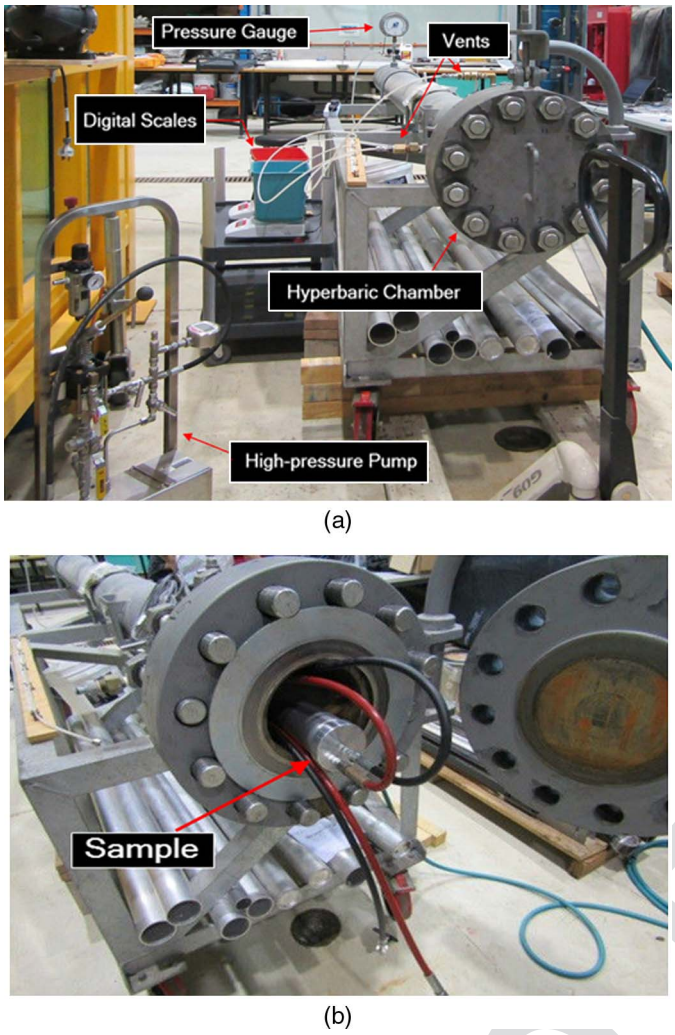

F2:1 **Fig. 2.** Experimental setup at Griffith University (images by Hassan
F2:2 Karampour): (a) hyperbaric chamber, high-pressure pump, scales,
F2:3 pressure gauge, and vents; (b) pipes and fittings

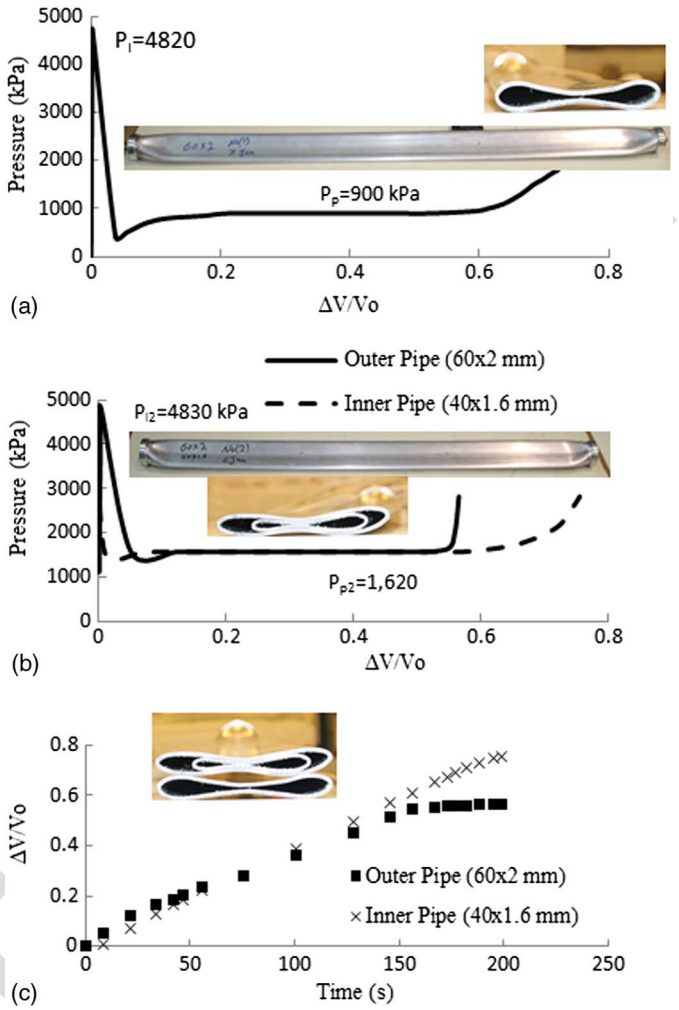

Fig. 3. Buckle propagation response inside the hyperbaric chamber: F3:1
(a) pressure versus normalized change in volume of the 60×2-mm F3:2
carrier pipe; (b) pressure versus normalized change in volume of F3:3
PIP-2; (c) normalized volume versus time for PIP-2 F3:4

Figs. 3–5 show the experimental results of the buckle propagation response. The pressure inside the chamber is plotted against the normalized change in volume of the carrier pipe (60×2 mm) of PIP-2 in Fig. 3(a). The chamber is gradually pressurized until the initiation pressure, P_I, is reached at which a section of the pipe collapses, resulting in a drastic drop in the chamber's pressure. The pressure is then maintained at the propagation pressure, P_p, with the dog-bone buckle shape longitudinally propagating along the length of the pipe. The buckle propagation response of the PIP-2 system is shown in Fig. 3(b). The change in system pressure is plotted against the normalized change in volume of the inner pipe, 40×1.6 mm, and the outer pipe, 60×2 mm (the space between the two pipes). Buckle is initiated first (P_{I2}) on the outer pipe; then the energy is released through ovalization of the outer pipe until the outer pipe touches the inner pipe.

Buckle initiation pressures, P_I and P_{I2}, have been shown to be closely related to geometric imperfections in the form of dents or ovality of the outer pipe (Karampour and Albermani 2014; Zheng et al. 2014). Because the main focus of the present study is buckle propagation pressures, the parameters affecting buckle initiation pressure are not discussed. Following the contact between the carrier pipe and the inner pipes of PIP-2, the inner pipe collapses and the buckle propagates longitudinally as long as the pressure is maintained at P_{p2}. When the stiff end caps fall within the vicinity of the buckle transition zone, a higher pressure is required to perpetuate the buckle which corresponds to the stiffening part of the PIP-2 response shown in Fig. 3(b). A dog-bone buckle shape similar to that observed in carrier pipe buckle propagation [Fig. 3(a)] was detected in the PIP-2 hyperbaric chamber test [Fig. 3(b)]. Changes in volume of the outer and inner pipes are plotted against the test time in Fig. 3(c). The time history shows an initial discharge from the outer pipe that is higher than that from the inner pipe. However, after the outer pipe touches the inner pipe at $\Delta V/V_o = 0.1$ [shown in Fig. 3(b)], discharge from the inner pipe is triggered and at $\Delta V/V_o > 0.2$ [shown in Fig. 3(c)] the discharge rate of the inner pipe exceeds that of the outer pipe. This shows that the collapse of the outer pipe is rapidly transferred to the inner pipe and is then followed by the longitudinal propagation of the buckle in both carrier and inner pipes. The rate of discharge in the carrier pipe and the inner pipe gradually decays as time lapses because of the introduction of the end caps in the buckle zone.

The hyperbaric chamber propagation buckling results for the 80×2-mm carrier pipe and the PIP-1 system are shown in Fig. 4. A small dent was made in the PIP-1 carrier pipe in the single-pipe test, which explains the lower buckle initiation pressure of the carrier pipe compared with that of PIP-2. As shown in Fig. 4(b),

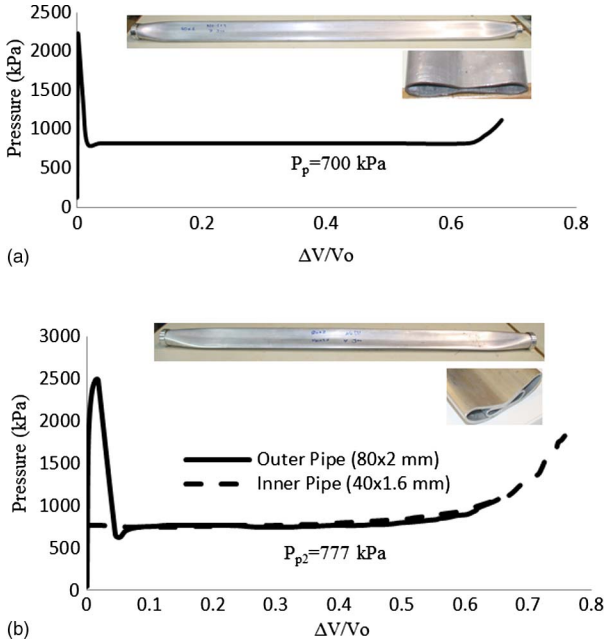

F4:1 **Fig. 4.** Buckle propagation response inside the hyperbaric chamber:
F4:2 (a) pressure versus normalized change in volume of the 80×2-mm
F4:3 carrier pipe; (b) pressure versus normalized change in volume for
F4:4 PIP-1

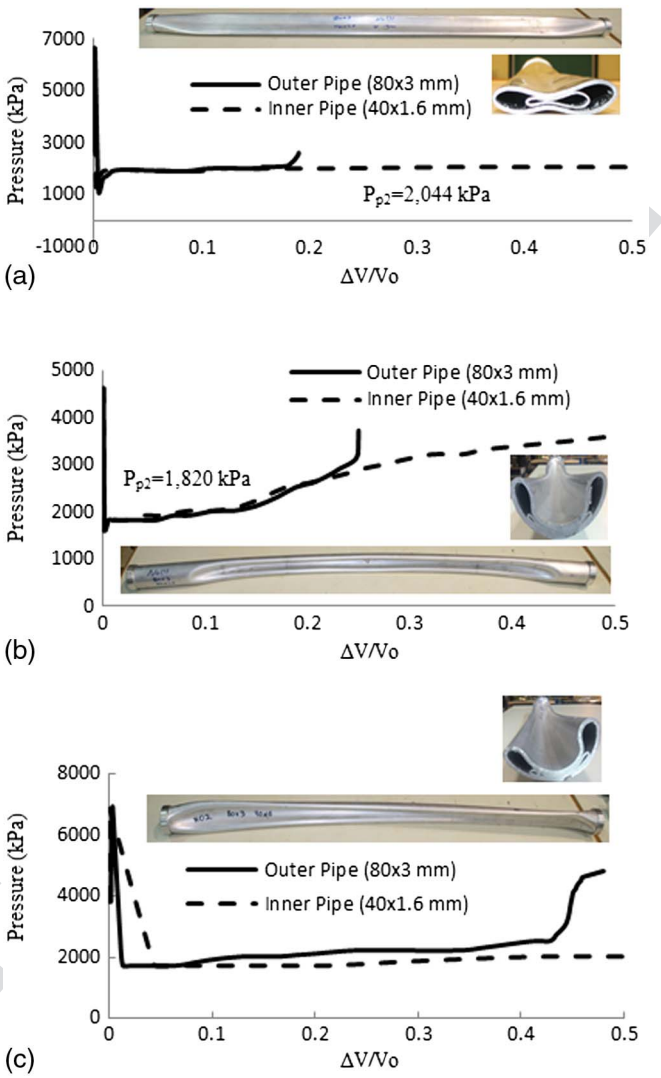

Fig. 5. Buckle propagation response inside the hyperbaric chamber: 10:1
F5:2 (a) buckle propagation response of PIP-3 (outer pipe: 80×3 mm; inner
F5:3 pipe: 40×1.6 mm) with dog-bone buckle shape; (b) buckle propaga-
F5:4 tion response of PIP-3 with confined buckle shape; (c) Buckle propa-
F5:5 gation response of PIP-3 showing interaction between dog-bone and
F5:6 confined buckle shape

following the collapse of the carrier pipe the pressure inside the chamber drops drastically until the carrier and inner pipes come into contact. Subsequently, a dog-bone buckle shape propagates along the PIP while the pressure is maintained at P_{p2}. Hyperbaric chamber tests of PIP-1 and PIP-2 were repeated twice each and no significant disparities were observed in the results.

Results for PIP-3 with $D_o/t_o = 26.7$ from three hyperbaric chamber tests are shown in Fig. 5. Unlike the responses of PIP-1 and PIP-2, three distinctive modes of buckling were observed in PIP-3: (1) the dog-bone buckle shape (flat mode), shown in Fig. 5(a); (2) the confined buckle shape (U mode), shown in Fig. 5(b); and (3) a combination of dog-bone and U-shaped buckle, shown in Fig. 5(c). The dog-bone mode of buckling is similar to the responses observed in PIP systems with high D_o/t_o values (PIP-1 and PIP-2). In this mode of failure, PIP-3 remains straight after failure and a flat mode of buckling propagates through its length; however, the deformed shape of the inner pipe is not symmetric in the cross section [shown in Fig. 5(a)].

In the second hyperbaric chamber test of PIP-3, shown in Fig. 5(b), a confined buckle shape is observed. The confined buckle mode is propagated along the length of the PIP while the pressure in the chamber is escalated followed by rapid discharge of water from the outer and inner pipes. This U-shape buckling mode was previously observed in confined-buckling tests of steel and aluminum tubes (Lee and Kyriakides 2004; Stephan et al. 2016). Stephan et al. (2016) performed an experimental investigation of the collapse of 3-m-long aluminum pipes inserted in a 2-m-long confining steel pipe. They observed a flat mode (dog-bone buckle shape) in the unconfined section of the aluminum pipe and a U-mode buckle shape in the confined section. Their experiments showed that within the studied range ($16 < D/t < 48$), the confined buckle shape consistently propagated at higher pressure compared with the dog-bone buckle shape. However, a comparison of Figs. 5(a and b) shows that in PIP-3 the U-shape buckling propagation ($P_{p2} = 1{,}820$ kPa) is initiated at a slightly lower pressure than the propagation pressure of the dog-bone buckle shape ($P_{p2} = 2{,}044$ kPa). In the third test, PIP-3 showed a dog-bone failure mode that had flipped into U mode. The average P_{p2} results from the hyperbaric chamber tests are summarized in Table 2.

Ring Squash Tests

Previous studies (Albermani et al. 2011; Kamalarasa and Calladine 1988) have shown that the RST is a satisfactory approach that gives a lower-bound estimate of buckle propagation pressure in single pipelines. The RST is conducted on a ring cut from the pipe specimen in such a way as to produce the dog-bone shape of the deformed pipe observed in the hyperbaric chamber. Fig. 6 shows the RST setup for a single pipe (60×2 mm). In this test, carried out in a universal testing machine, a short segment of the pipe with a length $l = 150$ mm (approximately $2.5D$) is squashed between two rigid cylinders of the same diameter and length as those of the pipe being tested. The two repeated tests are referred to

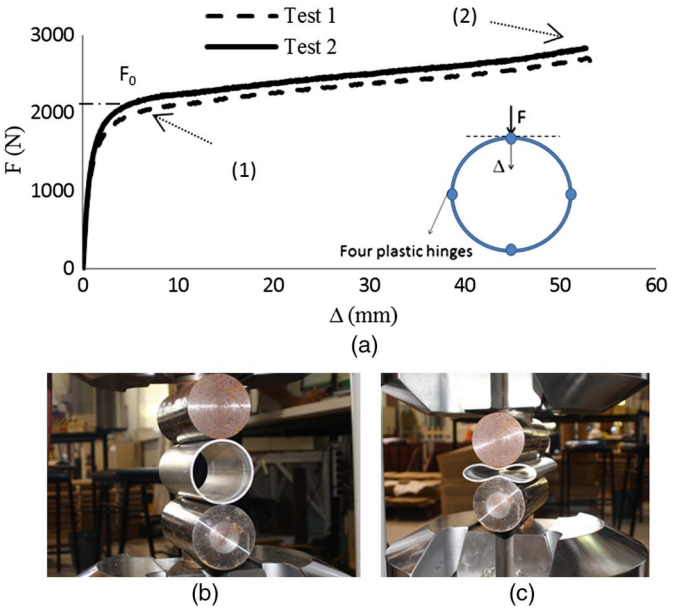

F6:1 **Fig. 6.** (a) Ring squash test results for single pipe (60×2 mm);
F6:2 (b) Collapse State 1; (c) Collapse State 2

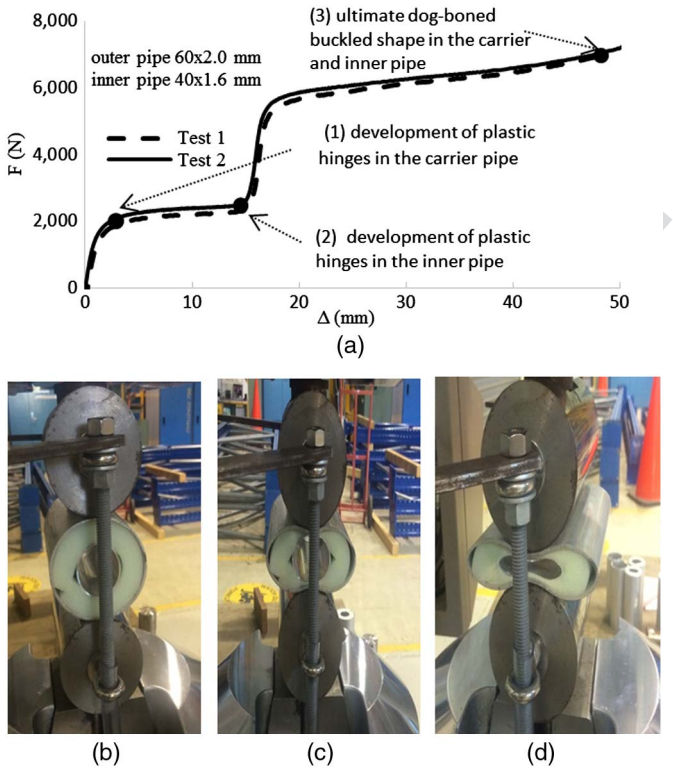

F7:1 **Fig. 7.** (a) Ring squash test results for PIP systems (outer pipe:
F7:2 60×2 mm; inner pipe: 40×1.6 mm); (b) Collapse State 1;
F7:3 (c) Collapse State 2; (d) Collapse State 3

as Tests 1 and 2 [Fig. 6(a)]. The force, F, required to compress the ring is plotted against the deformation of the pipe right under the load (Δ) in Fig. 6(a). The total energy dissipated in the RST process, U, can be evaluated by calculating the area under the force-displacement curve shown in Fig. 6(a). The pressure (P_{RST}) associated with the energy required for plastic deformation of the ring can be calculated from the following equation:

$$P_{\text{RST}} = \frac{U}{l \times \Delta A} \tag{10}$$

where ΔA = difference in area between the original circular shape and the final dog-bone configuration.

In this study, the RST has been modified to determine the propagation pressure of the PIP system. Short segments of the outer and inner pipes with lengths of $2.5D_o$ ($l = 150$ mm) are cut from the PIP specimen. The two pipes are held concentric during the test using soft foam in the space between them. The setup and the results of the RST for PIP-2 are shown in Fig. 7. The F-Δ relationships for the two repeated tests (Tests 1 and 2) agree well, as evident in Fig. 7(a). Collapse States 1 and 2 [Figs. 7(b and c)] correspond to the onset of plastic hinge development in the outer pipe and inner pipe, respectively. At the ultimate collapse state (State 3) shown in Fig. 7(d), four plastic hinges are developed in each pipe. Eq. (10) is used to determine the RST pressure of the PIP system (P_{p2}^{RST}). Two ring squash tests were conducted for each PIP system, and the averages of the results from the two tests are listed in Table 2 in form of $P_{p2}^{\text{RST}}/P_{p2}$. The ring squash test can be used to determine the yield stress, σ_Y, of the pipe using the following expression:

$$\sigma_Y = \frac{F_o D}{2Lt^2} \tag{11}$$

where F_o = load level at which the four plastic hinges shown in Fig. 6(a) are developed in the pipe wall. The effective yield stress calculated from the ring squash test implicitly accounts for the strain-hardening response of the material. Yield stresses, σ_Y, of the carrier pipes obtained from the ring squash tests are summarized in Table 1.

A confined-buckling ring squash test (CRST) protocol was proposed by Stephan et al. (2015) to investigate the buckling of a soft pipe encased in a stiff pipe. That procedure is modified here to model the U-shape buckle observed in the hyperbaric chamber tests of PIP-3. In the CRST, a 150-mm-long segment of PIP-3 is positioned inside a semicylindrical solid confinement of diameter D_o and diametrically compressed by a solid cylindrical indenter with a diameter of $(D_o - 2t_o - 2t_i)$. The softening part of the CRST response between Collapse States 1 and 2, shown in Fig. 8, corresponds to the development of the U-shape buckle in the outer pipe. The drop in response just before the end of Test 2 at Collapse State 3 is due to fracture of the pipe wall at one of the fold lines of the U shape. Results of the ring squash tests of the PIP systems and the confined ring squash test of PIP-3 (U-shape buckle) are summarized in Table 2.

Comparison of Analytical Solution and Experimental Results

Table 2 compares the analytical and experimental results. Pressures P_p and P_{p2} correspond to the buckle propagation pressures of the single pipe (carrier pipe) and the PIP system, respectively, obtained from the hyperbaric chamber tests. The variables $\hat{P}_p$ and $\hat{P}_{p2}$ refer to the analytical solutions proposed by Kyriakides and Vogler (2002) for the propagation buckling pressure of the single pipe and the PIP system given in Eqs. (2) and (3), respectively. The analytical expressions derived in the current study for propagation buckling pressure of single pipes and PIP systems are listed in Table 2 as $\tilde{P}_p$ and $\tilde{P}_{p2}$, which correspond to Eqs. (6) and (9), respectively. The propagation pressures from the RSTs of the PIP systems (and the CRST for PIP-3) are represented as P_{p2}^{RST}. To

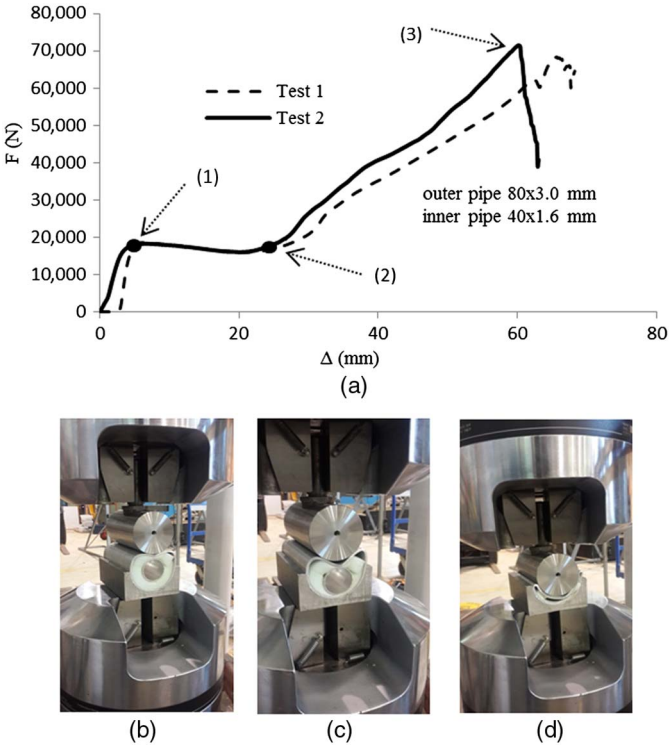

F8:1 **Fig. 8.** (a) Confined ring squash test results for PIP systems (outer
F8:2 pipe: 80 × 3 mm; inner pipe: 40 × 1.6 mm; (b) Collapse State 1;
F8:3 (c) Collapse State 2; (d) Collapse State 3

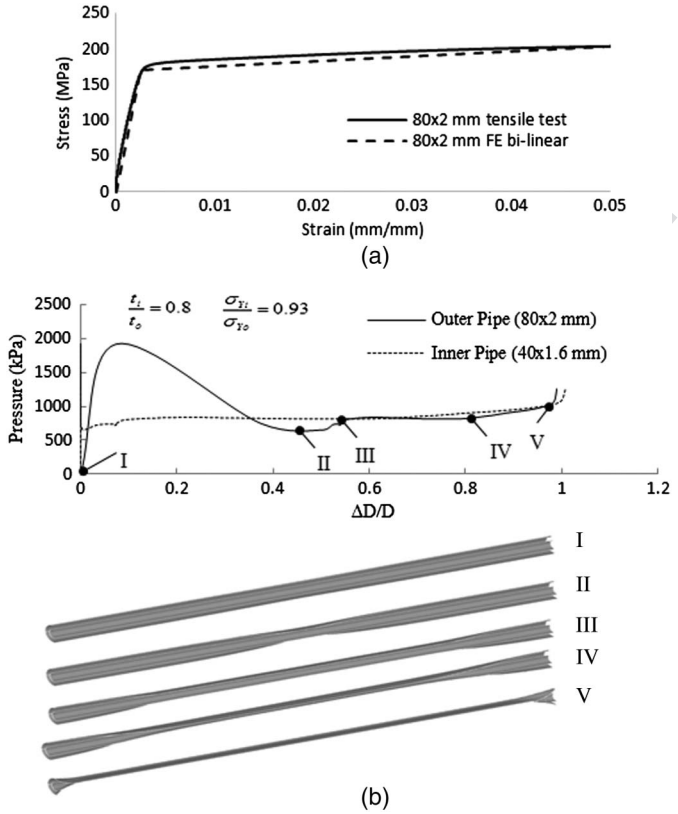

Fig. 9. (a) Experimental and FE stress-strain curves; (b) FE results showing pressure against normalized ovality and corresponding PIP-1 deformed shapes

make meaningful comparisons, the analytical and ring squash results are normalized to the hyperbaric chamber results.

As represented in Table 2, the analytical solutions provide lower bounds for the propagation buckling of the single pipes and PIP systems. Propagation pressures of single pipes predicted from the analytical solutions, $\hat{P}_p$ and $\tilde{P}_p$, are from 55 to 79% of the propagation pressure, P_P, from the hyperbaric chamber results. In single pipelines, the difference between the analytical and hyperbaric chamber results decreases with a corresponding reduction in the D_o/t_o ratio, whereas in PIP systems the difference between the analytical and hyperbaric chamber results increases with a corresponding decrease in the D_o/t_o ratio. Comparison of the analytical and experimental results in Table 2 indicates that Eq. (9) predicts the propagation buckling of the PIP system better than Eq. (3) regardless of the D_o/t_o ratio.

It can be further observed from Table 2 that the ratio of propagation pressure obtained from the ring squash tests (P_{p2}^{RST}) to those from the hyperbaric chamber tests varies from 0.49 to 0.76 for the PIP systems. Albermani et al. (2011) and Kamalarasa and Calladine (1988) suggested average ring squash–to–hyperbaric chamber pressure ratios of approximately 0.73 for single pipes. It appears that the ring squash test provides a highly conservative prediction of the propagation pressure of PIP systems with low D_o/t_o ratios. Interestingly, the propagation pressure of PIP-3 from the CRSTs (U-shape buckle) is only 2% lower than the U-shape propagation pressure from the hyperbaric chamber tests.

Finite-Element Analysis

Finite-element simulation of 1.6-m-long samples of the PIP systems used in the hyperbaric chamber tests were conducted using ANSYS. Thin four-node shell elements (181) were used to model the carrier pipe and the inner pipe. Frictionless contact and target elements (174 and 170) were used in three pairs to define the nonlinear contact between the carrier and inner pipes and the inner surfaces of the inner-pipe wall. Because of symmetry, a one-half model of the pipe wall (180°) was discretized using 24 elements in the circumferential direction with seven integration points through the thickness of the carrier pipe and the inner pipe. To better facilitate the nonlinear analysis, a small ovalization ratio Ω [Eq. (13)] of 0.5% was introduced at midlength on the carrier pipe in the FE model

$$\Omega = \frac{D_{\max} - D_{\min}}{D_{\max} + D_{\min}} \tag{12}$$

where $D_{\max}$ and $D_{\min}$ = maximum and minimum outer diameters along the pipe length, respectively. The nodes at either end of the PIP systems were restrained from translation in all directions. A von Mises elastoplastic (bilinear) material definition with isotropic hardening was adopted. The modulus of elasticity, E, and tangent modulus, E', used in the FE models are also listed in Table 1 and are based on the stress-strain curves obtained from the tensile longitudinal coupons taken from the pipe wall shown in Fig. 9(a). The yield stresses used in the FE models are taken from the ring squash tests using Eq. (11) and are listed in Table 1 as σ_{Yo} and σ_{Yi} for the outer pipe and inner pipe, respectively. The FE predictions for PIP-2 and PIP-3 propagation pressure in Table 2 represent 86 and 96%, respectively, of the experimental results. However, the propagation pressure obtained from the FE analysis overestimates the experimental results for PIP-1.

The pressure response and the deformed shape of PIP-1 and PIP-2 from the FE analyses are shown in Figs. 9(b) and 10,

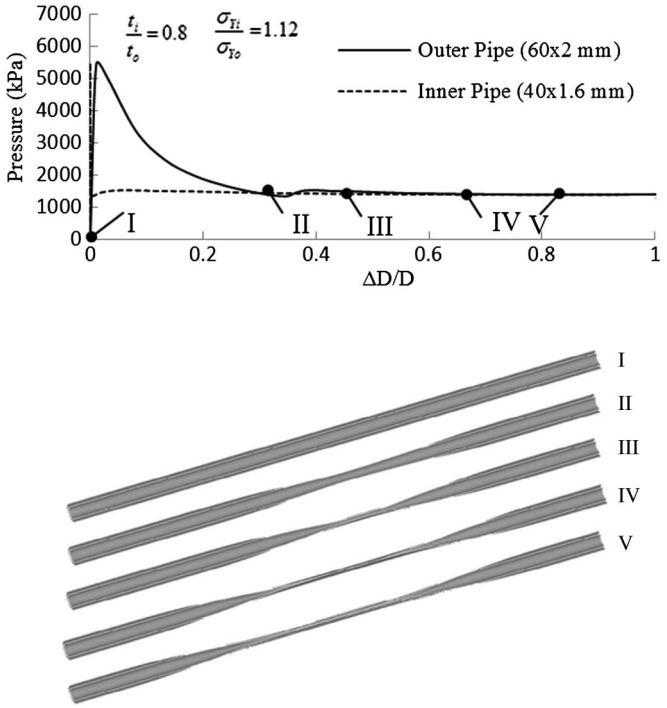

F10:1 F10:2 **Fig. 10.** FE results showing pressure against normalized ovality and corresponding PIP-2 deformed shapes

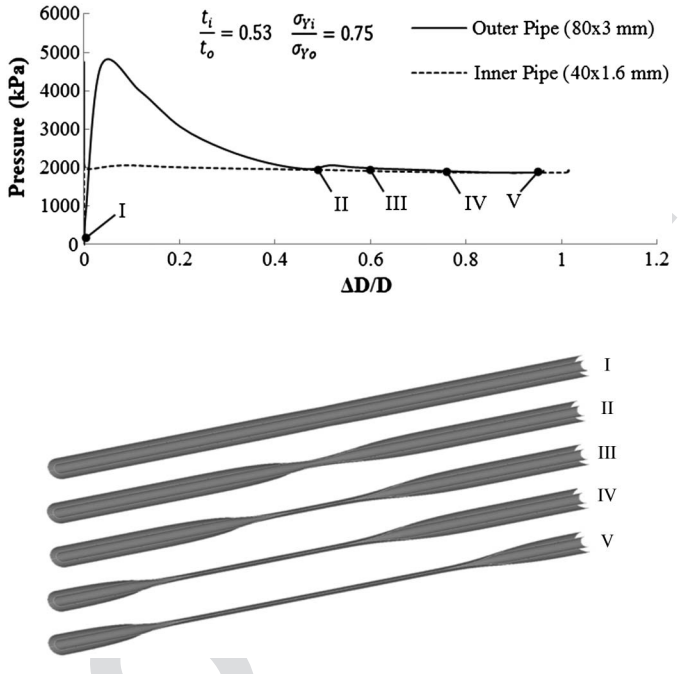

F11:1 F11:2 **Fig. 11.** FE results showing pressure against normalized ovality and corresponding PIP-3 deformed shapes

respectively. The pressure is plotted against the normalized ovalization of the carrier and inner pipes ($\Delta D/D$). By increasing the hydrostatic pressure, the carrier pipe of PIP-1 in Fig. 9(b) gradually deforms from an intact shape (Stage I) to a deformed shape (Stage II). At this stage, the outer and inner pipes come into contact and a small deformation is observed in the inner pipe. The local collapse in the inner pipe is arrested, which is followed by a slight increase in pressure. The collapse is then propagated in the outer pipe until detained by the end caps, as depicted in the deformed shape (Stage III). In the vicinity of the end-caps, a higher pressure is required to perpetuate the collapse in the outer pipe. However, the increase in pressure causes a collapse in the inner pipe at the pressure level (Stage IV) and initiates a buckle that is propagated through the length. This mode of buckling, in which the collapse propagates over the inner pipe, was reported by Gong and Li (2015) and Kyriakides (2002) as occurring in a PIP system where the inner pipe is stiffer (has larger thickness and yield stress) than the outer pipe. However, in the present study this buckling mode was observed in PIP-1, in which the inner pipe is softer than the outer pipe.

The buckling response of PIP-2 is shown in Fig. 10. Following the touchdown (Stage II), the pressure is slightly increased and the collapse is propagated in the outer pipe in a length of approximately $8D$. The inner tube is then collapsed, and buckle propagation is distributed along the length of PIP-2 (Deformation Stages IV and V). Knowing that the inner pipes in PIP-1 and PIP-2 are identical, comparison of the buckling responses in Figs. 9 and 10 demonstrates that the collapse pressure of the inner pipe in PIP-2 is significantly higher (68%) than that of the inner pipe in PIP-1. This difference in collapse pressures of identical inner pipes in different PIP systems is an important factor in the design of PIP systems where the inner pipe is intended to safely carry the internal fluids.

The pressure response and the deformed shape of PIP-3 from the FE analyses are shown in Fig. 11. This dog-bone buckle mode is similar to the failure mode shown in Fig. 5(a), which was obtained from the hyperbaric chamber tests. To explain the U-shape buckling modes observed in the hyperbaric chamber tests of PIP-3, shown in Figs. 5(b and c), some scenarios were assumed in the FE models. To account for potential manufacturing defects, nonconcentric PIP models were created and the inner pipe was located 1–5% off-center from the outer pipe in the horizontal and vertical directions. No significant change in propagation pressure of the eccentric PIP systems was observed, and all FE models exhibited dog-bone failure modes.

To account for the rigid foundation boundary condition in the nonlinear FE model, the nodes at the very bottom of the carrier pipe were constrained against translation along the left one-third of PIP-3's length. The FE response of the PIP-3 model is shown in Fig. 12. Buckle propagation is triggered in the middle of PIP-3 and is then propagated in a dog-bone shape to the right of the specimen. The pressure required to propagate this dog-bone buckle mode, shown in Stage III in Fig. 12, is close to the pressure measured in the hyperbaric chamber test shown in Fig. 5(c). When the dog-bone buckle mode reaches the end cap at the right end of the PIP system, the U-shape mode is triggered at the left end of PIP-3, as shown in Stage IV. The U-shape buckle then propagates toward the left end cap and is accompanied by an increase in system pressure, as suggested by the transition from Stage IV to Stage V in Fig. 12.

To further investigate nonlinear buckling response, another FE model for PIP-3 with different boundary conditions was created. The nodes at the very bottom of the carrier pipe were restrained from translation along the entire length of the PIP system. The FE results are shown in Fig. 13 and depict a U-shape buckle that is initiated in the carrier pipe and quickly transferred to the inner pipe. The propagation pressure and failure mechanism of PIP-3 from the FE results, shown in Fig. 13, are similar to the response observed in the hyperbaric chamber test shown in Fig. 5(b). The global curvature observed in the inner pipe in Stage V of the FE response was also detected in the failed PIP-3 specimen from the hyperbaric chamber test. It is worth mentioning that the collapse pressure of the inner pipe in the U-shape buckling mode of Fig. 13

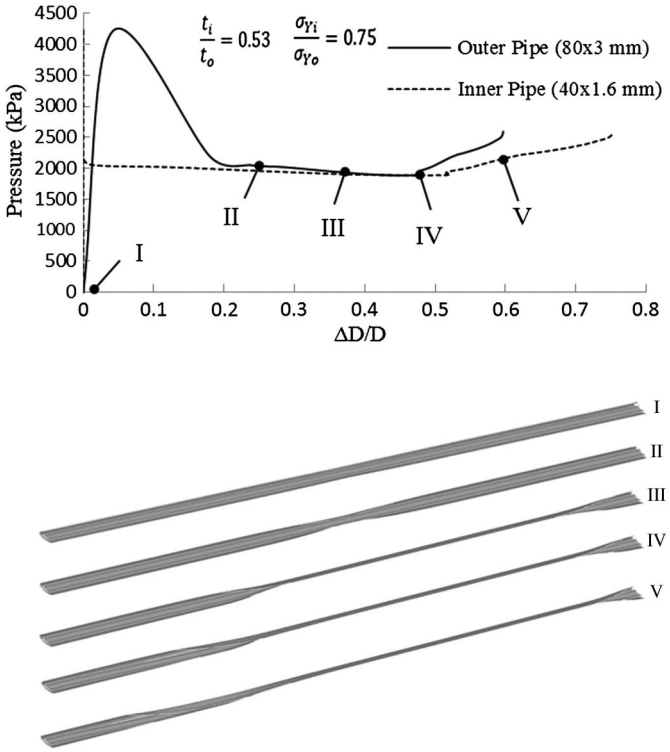

F12:1 **Fig. 12.** FE results showing pressure against normalized ovality and
F12:2 corresponding PIP-3 deformed shapes with bottom constraint on a third
F12:3 of the length

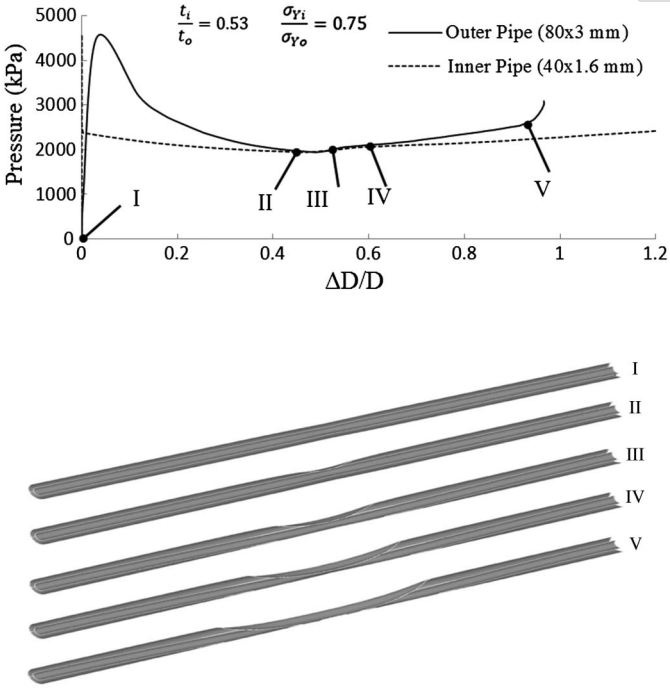

F13:1 **Fig. 13.** FE results showing pressure against normalized ovality and
F13:2 corresponding PIP-3 deformed shapes with bottom constraint along the
F13:3 entire length

is higher than the corresponding collapse pressures in the dog-bone and flip-flop modes shown in Figs 11 and 12, respectively.

The length of the transition zone in the carrier pipes (l_t) from the finite-element models are listed in Table 3. Kamalarasa and

Table 3. FE Results for Transition Lengths of Single Pipes and PIP Systems

		Carrier pipe			Pipe-in-pipe (FE)		
Identifier	D_o/t_o	$\hat{l}_t$ (mm) Eq. (10)	l_t (mm) FE	$\frac{l_t}{D_o}$	$\frac{l_{t2}^i}{l_t}$	$\frac{l_{t2}^F}{Do}$	T3:2 T3:1
PIP-1	40.0	644	698	8.72	1.02	19.26	T3:3
PIP-2	30.0	418	487	8.11	0.79	12.87	T3:4
PIP-3[a]	26.7	526	611	7.64	0.90	10.77	T3:5

[a]Dog-bone buckle shape.

Calladine (1988) performed a dimensional analysis and found the following expression for the length of the transition zone in single pipes:

$$\hat{l}_t = 3.6\sqrt{\frac{r^3}{t}} \tag{13}$$

Carrier pipe transition lengths obtained from the FE models are on average 13% greater than those predicted by Eq. (13). The average transition length of a single pipe (approximately $8D$) obtained from the current FE analysis is close to $10D$, as reported by Chater and Hutchinson (1984), and $6D$, as reported by Albermani et al. (2011). With regard to the PIP systems, two distinctive transition lengths can be defined from the FE results: one corresponds to the onset of first contact between the carrier pipe and the inner pipe (l_{t2}^i), and the other represents the length of the transition zone in full dog-bone buckle propagation mode in the PIP system (l_{t2}^F). The transition lengths l_{t2}^i and l_{t2}^F are important parameters for efficient design of buckle arrestors in PIP systems (Kyriakides and Netto 2004). A value of $l_{t2}^i/l_t > 1$ essentially means that buckling is propagated along the carrier pipe without affecting the inner pipe, which is important from a design point of view. The full propagation transition lengths of the PIP systems (l_{t2}^F) listed in Table 3 range from 10 to $20D_o$ with an average of $14D_o$—almost twice the corresponding transition lengths in single pipes.

Conclusions

Experimental, analytical, and FE results for buckle propagation of pipe-in-pipe systems were presented. Hyperbaric chamber tests were conducted on 1.6-m-long aluminum pipe-in-pipe systems. Confined buckling and flip-flop buckling modes were discovered in the hyperbaric chamber test of PIP-3 which had not been reported in the literature. These buckling modes occurred at propagation pressures close to that observed in a dog-bone buckle shape. Based on observations from the hyperbaric chamber test results of PIP systems, RST and CRST protocols were proposed. Nonlinear FE analyses were conducted and verified against the hyperbaric chamber tests. The FE models provided valuable information about the buckling modes and progress in carrier and inner pipes. The following conclusions can be drawn from the present study:

- The modified analytical solution suggested in this study accounts for the D_i/D_o ratio and provides more accurate predictions of PIP propagation buckling pressure compared with previous analytical equations;
- The RST and CRST provide lower-bound estimates of PIP propagation pressure; for PIP systems with intermediate D_i/t_o values, the RST pressure is almost half the propagation pressure as measured by the hyperbaric chamber tests; however, the CRST

result is very close to the confined buckling propagation pressure obtained from the hyperbaric chamber tests;

- The nonlinear FE results suggest that the new buckling modes observed in PIP-3 are in accordance with different boundary conditions that the carrier pipe may adopt;
- The FE results show that the length of the transition zones of PIP systems are almost twice the corresponding lengths in single pipes; and
- The present study focused on the propagation pressure of PIP systems with identical inner pipes but different carrier pipes; the FE results presented in Figs. 9–13 showed substantial differences in the collapse pressure of the inner pipes in different PIP systems; further investigation is recommended to fully understand the failure mechanisms of the inner pipe of PIP systems.

Acknowledgments

The authors are grateful for the SEED funding received from the Griffith School of Engineering, Griffith University.

References

Albermani, F., Khalilpasha, H., and Karampour, H. (2011). "Propagation buckling in deep sub-sea pipelines." *Eng. Struct.*, 33(9), 2547–2553.

ANSYS 16.1 [Computer software]. ANSYS, Canonsburg, PA.

Bai, Y., and Bai, Q. (2005). *Subsea pipelines and risers*, Elsevier, London.

Bokaian, A. (2004). "Thermal expansion of pipe-in-pipe systems." *Mar. Struct.*, 17(6), 475–500.

Chater, E., and Hutchinson, J. W. (1984). "On the propagation of bulges and buckles." *J. Appl. Mech.*, 51(2), 269–277.

Gong, S., and Li, G. (2015). "Buckle propagation of pipe-in-pipe systems under external pressure." *Eng. Struct.*, 84(7), 207–222.

Jukes, P., Eltaher, A., Sun, J., and Harrison, G. (2009). "Extra high-pressure high-temperature (XHPHT) flowlines: Design considerations and challenges." *Proc., ASME 28th Int. Conf. on Ocean, Offshore and Arctic Engineering*, ASME, New York, 469–478.

Kamalarasa, S., and Calladine, C. R. (1988). "Buckle propagation in submarine pipelines." *Int. J. Mech. Sci.*, 30(3–4), 217–228.

Karampour, H., and Albermani, F. (2014). "Experimental and numerical investigations of buckle interaction in subsea pipelines." *Eng. Struct.*, 66(5), 81–88.

Karampour, H., and Albermani, F. (2015). "Buckle interaction in textured deep subsea pipelines." *Ships Offshore Struct.*, 11(6), 1–11.

Karampour, H., Albermani, F., and Gross, J. (2013a). "On lateral and upheaval buckling of subsea pipelines." *Eng. Struct.*, 52, 317–330.

Karampour, H., Albermani, F., and Major, P. (2015). "Interaction between lateral buckling and propagation buckling in textured deep subsea pipelines." *Proc., ASME 2015 34th Int. Conf. on Ocean, Offshore and Arctic Engineering*, ASME, New York, V003T002A079–V003T002A079.

Karampour, H., Albermani, F., and Veidt, M. (2013b). "Buckle interaction in deep subsea pipelines." *Thin Walled Struct.*, 72, 113–120.

Kyriakides, S. (2002). "Buckle propagation in pipe-in-pipe systems, I: Experiments." *Int. J. Solids Struct.*, 39(2), 351–366.

Kyriakides, S., and Babcock, C. D. (1981). "Experimental determination of the propagation pressure of circular pipes." *J. Pressure Vessel Technol.*, 103(4), 328–336.

Kyriakides, S., Babcock, C. D., and Elyada, D. (1984). "Initiation of propagating buckles from local pipeline damages." *J. Energy Res. Technol.*, 106(1), 79–87.

Kyriakides, S., and Netto, T. A. (2004). "On the dynamic propagation and arrest of buckles in pipe-in-pipe systems." *Int. J. Solids Struct.*, 41(20), 5463–5482.

Kyriakides, S., and Vogler, T. J. (2002). "Buckle propagation in pipe-in-pipe systems, II: Analysis." *Int. J. Solids Struct.*, 39(2), 367–392.

Lee, L. H., and Kyriakides, S. (2004). "On the arresting efficiency of slip-on buckle arrestors for offshore pipelines." *Int. J. Mech. Sci.*, 46(7), 1035–1055.

Mesloh, R. E., Sorenson, J. E., and Atterbury, T. J. (1973). "Buckling and offshore pipelines." *Gas Magazine*, 7, 4.

Palmer, A. C., and Martin, J. H. (1975). "Buckle propagation in submarine pipelines." *Nature*, 254(5495), 46–48.

Stephan, P., Love, C., Albermani, F., and Karampour, H. (2016). "Experimental study on confined buckle propagation." *Adv. Steel Constr.*, 12(1), 44–54.

Vaz, M. A., and Patel, M. H. (1999). "Lateral buckling of bundled pipe systems." *Mar. Struct.*, 12(1), 21–40.

Wang, Z., Chen, Z., and Liu, H. (2015). "Numerical study on upheaval buckling of pipe-in-pipe systems with full contact imperfections." *Eng. Struct.*, 99(4), 264–271.

Zheng, J., Palmer, A., Brunning, P., and Gan, C. T. (2014). "Indentation and external pressure on subsea single wall pipe and pipe-in-pipe." *Ocean Eng.*, 83(25), 125–132.